CHALMERS

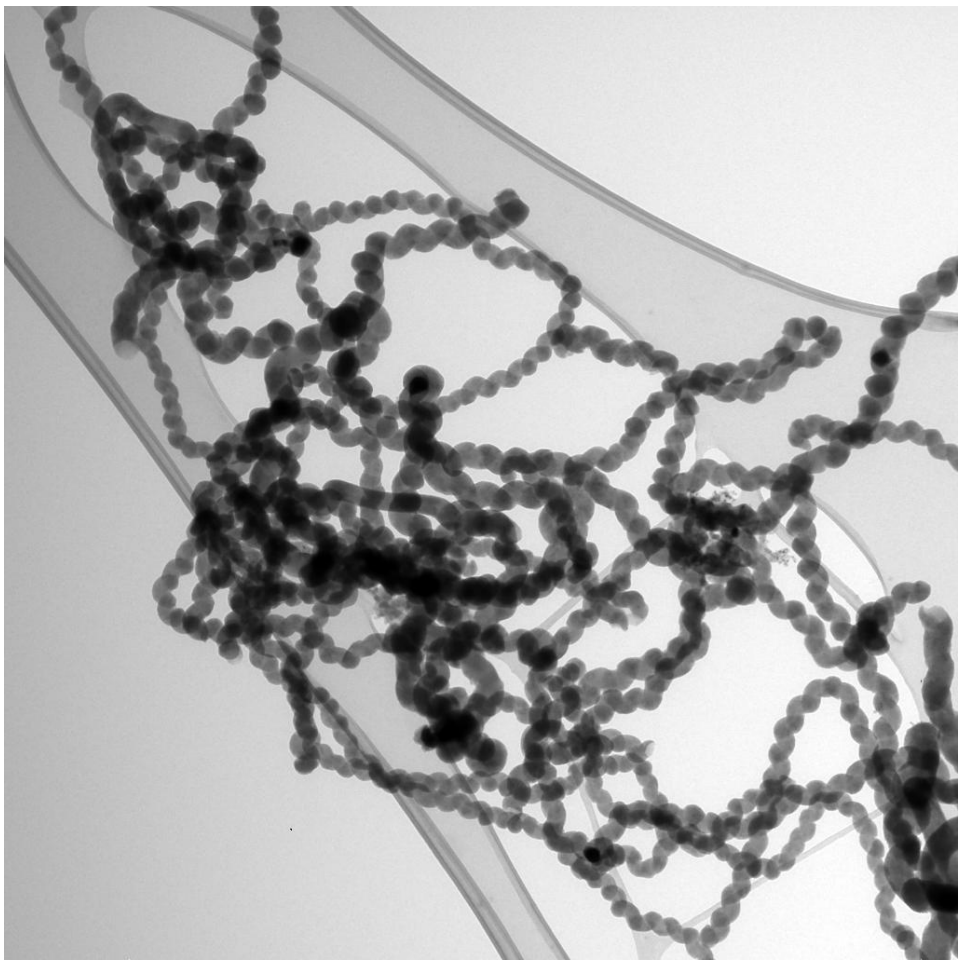

Tackling the Volume Increase Problem of Lithium-Sulfur Batteries During Cycling

Master's Thesis in Applied Physics

SIMON ANDERSSON

Department of Applied Physics
Condensed Matter Physics
Chalmers University of Technology
Gothenburg, Sweden 2014

Tackling the Volume Increase Problem of Lithium-Sulfur Batteries During Cycling

Thesis for the degree Master of Science

SIMON ANDERSSON

Department of Applied Physics
Condensed Matter Physics
Chalmers University of Technology
Gothenburg, Sweden 2014

Tackling the Volume Increase Problem of Lithium-Sulfur Batteries During Cycling
Thesis for the degree Master of Science
Simon Andersson

Condensed Matter Physics
Department of Applied Physics
Chalmers University of Technology
SE-412 96 Gothenburg, Sweden
Telephone:+46 (0)31 772 1000

Cover: Transmission electron microscopy image of synthesized helical carbon nanofibers.

Printed at Chalmers Reproservice
Gothenburg, Sweden 2014

Tackling the Volume Increase Problem of Lithium-Sulfur Batteries During Cycling

SIMON ANDERSSON
Department of Applied Physics
Chalmers University of Technology

Abstract

Lithium-sulfur cells are of big interest due to their high potential as a successor of Li-ion batteries. They have a significantly higher teoretical capacity than todays Lithium-ion batteries and have been of high interest for several years. However, they still suffer from several problems, especially from poor cyclability. One of the reasons for the low cyclability is the large volume increase of the cathode during cycling. The volume expansion and contraction requires the cathode to withstand the induced forces.

In this thesis the synthesis and use of helical carbon nanofibers (HCNFs) as a potential flexible cathode is explored. Due to the HCNFs very special shape, that reminds of a telephone cord, the cathode is believed to be able to "breath". HCNFs are synthesized by chemical vapor deposition and activated with potassium hydroxide to increase the porosity. The electrodes are prepared by mixing elemental sulfur and HCNFs by a simple melt-diffusion approach. The activation significantly increases the porosity of the HCNFs. The specific capacity is highly increased in the activated HCNFs compared to the prestine HCNFs at low discharge rates. The capacity is almost twice as high in the activated HCNFs compared to activated multi-walled carbon nanotubes. The activated HCNFs retain a specific discharge capacity above 560 mAh/g over 50 cycles with a coulombic efficiency of 97.0 %, which is similar to published results with straight nanofibers.

Acknowledgements

I would like to express my gratitude to Professor Aleksandar Matic for giving me the opportunity to work on this project. I would also like to express my very great appreciation to my supervisor Florian Nitze for his exemplary guidance and assistance throughout the project. I also take this opportunity to express a deep gratitude to Professor Anders Palmqvist and Thomas Wågberg and all other people, both from Umeå University and Chalmers, who have helped me during my project. My special thanks goes to Robin Sandström for sending new fibers whenever in need. Finally, I wish to thank Ida-Maria for her support and encouragement throughout the project.

Simon Andersson, Göteborg 25th of May 2014

Contents

Common abbreviation

2:1, 3:1	-	Activation ratio
BET	-	Brunauer Emmett Teller (gas adsorption analysis)
CV	-	Cyclic voltammetry
CVD	-	Chemical vapour deposition
EDX	-	Energy-dispersive X-ray Spectroscopy
FFT	-	Fast fourier transform
HCNFs	-	Helical carbon nanofibers
MWCNTs	-	Multi-walled carbon nanotubes
PVDF	-	Polyvinylidene fluoride (binder)
S-HCNFs	-	Sulfur impregnated HCNFs
SEM	-	Scanning electron microscopy
TEM	-	Transmission electron microscopy
TGA	-	Thermogravimetric analysis

1

Introduction

There is a high interest in the world for better batteries due to many reasons. One of the most commonly discussed problem is probably to make the commercialization of electric cars possible. The local environment could be significantly improved and in combination with sustainable electricity production the carbon dioxide emissions can be decreased by replacing combustion engines with electric ones. The availability of fossil fuels is also limited which makes it inevitable to replace gasoline cars. Another reason is the varying generation of electric power from renewable sources caused by varying weather, seasons and day time. The need of storing energy from the peak of production to the peak of consumption is therefore of tremendous interest to increase the utilization of sustainable energy plants [1]. Other reasons are the increasing uses of portable electronic devices and also better security backup systems in safety purposes. Todays standard Li-Ion batteries are close to reach their theoretical capacity limit and thus a new technology is needed.

1.1 The Lithium/Sulfur cell

The lithium/sulfur battery has been of great interest in the last three decades due to the theoretically high energy density around 3-5 times higher than today's lithium/ion batteries. However there are still several problems associated with the lithium/sulfur technology. The lithium/sulfur cell consist of a lithium and a sulfur electrode. During discharge lithium ions are transported through the electrolyte to the sulfur electrode. Lithium sulfides are formed at the cathode and the final product, lithium sulfide, has 79.2 % larger volume than pure sulfur [2]. The large volume increase can cause the cathode to crack and thus the mechanical properties of the sulfur electrode are of great importance. Due to the low conductivity of sulfur the electrode is usually mixed with different kinds of carbon materials that act as a conductive matrix. Another problem of the lithium/sulfur cell is dissolution of polysulfides in the electrolyte which causes problems such as decrease in capacity during cycling, high self-discharge and reduced

safety [2].

Previously, considerable research effort has been focused on creating different carbon structures that contain sulfur and at the same time prevent its dissolution into the electrolyte. The encapsulation of sulfur has been done with many different methods. For example by impregnating carbon nanofibers [3] and different kinds of mesoporous carbons [4, 5] with sulfur or by filling of hollow carbon nanofibers with sulfur [6].

1.2 Project Objectives

The purpose of this study is to investigate the potential of using helical carbon nanofibers (HCNFs) as a cathode material in lithium/sulfur cells to improve the cyclability. The flexibility of HCNFs are believed to better handle the volume expansion of the active material in the cathode compared to other carbon based structures thanks to the special shape. HCNFs are synthesized by chemical vapour deposition on palladium catalyst particles and the HCNFs are activated by using potassium hydroxide to increase their porosity. HCNFs are sulfur impregnated by melt diffusion, where HCNFs and sulfur are mixed and heated to suitable temperatures. The electrodes are tested in coin cells and by performing potentiometry cycling. Characterization is done by transmission electron microscopy (TEM), scanning electron microscopy (SEM), thermogravimetric analysis (TGA) and Brunauer–Emmett–Teller (BET) analysis.

2

Theory

2.1 The Galvanic Cell

Galvanic cells, batteries or electrochemical devices transform energy from chemical to electrical energy and vice versa. Each cell consists of three essential parts; anode, cathode and electrolyte. In general, the anode material loses electrons (oxidation) and the cathode material gains electrons (reduction) during discharge. The anode and the cathode are soaked in the electrolyte which has the purpose to conduct ions but not electrons. The electrolytes are connected by a salt bridge or with a separator that allows exchange of ions and avoids short-cut. The electrodes are connected with an external circuit that conducts electrons and the passing electrons must be matched by the charges from the transported ions in the electrolyte. This implies that the current can be controlled by adding a load to the external circuit. The chemical force that creates the flow of ions, and the resulting electrons, in the battery is due to the difference in chemical potential/Gibbs free energy between the anode and the cathode [1]. The theoretical cell voltage of a cell can easily be determined by calculating the difference in standard potential of the two reacting materials. A complete battery generally consists of one or several cells. The cells can be arranged in parallel to increase capacity or in series to increase voltage. An illustration of a galvanic cell is shown in figure 2.1.

2.2 The Lithium/Sulfur cell

The lithium/sulfur battery has a theoretical energy density of 2600 Wh/Kg and a theoretical specific capacity of 1675 mAh/g both calculated per mass elemental sulfur [7]. The lithium/sulfur cell consists of a lithium anode and a cathode containing sulfur. During discharge lithium ions are transported to the sulfur cathode to finally form Li_2S. This process is rather complicated and takes place in several steps as shown in equation 2.1 [2].

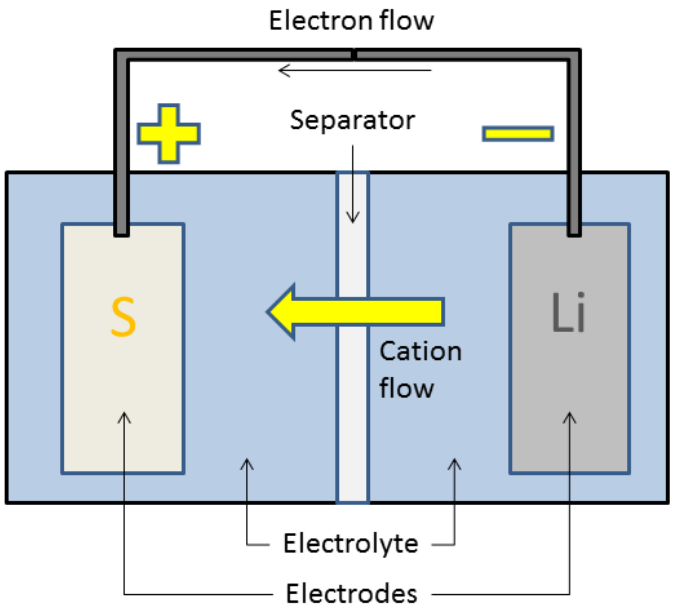

Figure 2.1: Schematic of a lithium/sulfur cell at discharge.

$$S_8 \rightarrow Li_2S_8 \rightarrow Li_2S_6 \rightarrow Li_2S_4 \rightarrow Li_2S_2 \rightarrow Li_2S \tag{2.1}$$

The formation of Li_2S in the cathode corresponds to a volumetric increase at discharge of 79.2 % [2] compared to elemental sulfur. Due to the fact that sulfur is poorly conducting, carbon structures are usually mixed with the sulfur to make it conductive. The sulfur is usually introduced into different allotropes of carbon by impregnation or encapsulated into different carbon structures. To benefit from the specific capacity advantages of the lithium/sulfur cell at least 70 wt% of the cathode should be sulfur [2].

Another problem with lithium/sulfur cells are the so called shuttle reactions, which are due to the formation of soluble polysulfides in the substeps towards Li_2S ($Li_2S_n, n = 4-8$) [8] that are dissolved in the electrolyte. Both Li_2S and Li_2S_2 are hardly soluble at all in electrolytes whereas polysulfides can be solved to quite large extent in many electrolytes [2]. The shuttle reactions decrease the capacity of lithium/sulfur batteries, especially over cycling. Polysulfides formed at the cathode are, undesirably, transported to the anode where they react with the lithium anode. The polysulfides can then be transported back to the cathode where they become reoxidized and the process starts over again [7]. This process induces self-discharge. The polysulfides transported to the anode can also form Li_2S at the anode which is non-soluble and thus capacity is permanently lost. These processes are thought to be avoided if the sulfur is encapsulated deep enough into the carbon structure so that the contact between the polysulfides and the electrolyte is minimized. However, it is self-evident that the contact to the electrolyte

is essential for the battery to function therefore this complicates the situation.

2.3 Previous Work

Considerable efforts have previously been focused on different carbon structures and different encapsulation approaches for sulfur. For example, H. Wang et al. wraped graphene around sulfur coated carbon nanofibers [9], J. Schuster et al. impregnated ordered mesoporous carbon nanoparticles with sulfur [4] and N. Jayaprakash et al. filled hollow carbon capsules with sulfur [5], but still the problem of capacity fading over a large amount of cycles remains. Problematic is also that the added carbon decreases the total specific capacity due to increased fraction of non-active material.

G. Zheng et al. filled hollow carbon nanofibers with sulfur [6]. The contact between the sulfur and the electrolyte was limited to the two openings of the fibers and the hollow structure provided large space for expansion. At low rate, 0.2 C, the specific capacity was more than 900 mAh/g after 30 cycles and 730 mAh/g after 150 cycles, where 1 C is defined as the current that theoretically discharges the battery in one hour and the specific capacity is per weight of sulfur. Z. Deng et al. instead used vapor grown carbon fibers (VGCF) where the sulfur was embedded into small pores created/enlarged by activation with potassium hydroxide (KOH) [3]. They claimed that the existence of pores decreased the polysulfide shuttle. However the specific energy still decreased from 928 mAh/g to 408 mAh/g after 80 cycles. The KOH that was mixed with the VGCF at a ratio of 1:4 did increase the pore diameter mostly in the range of 3 – 30 nm. Also Ran Elazari et al. obtained promising results by sulfur impregnation of activated carbon fibers in a similar manner as Deng et al. but by using a commercial activated binder free carbon fiber cloth [10]. They managed to keep 800 mAh/g after 80 cycles. Another route to encapsulate sulfur into porous carbon nanofibers has been persued by Liwen Ji et al. [11]. They used a solution-based chemical reaction-deposition method and claimed that this technique provides intimate contact between the sulfur and the carbon nanofibers. They managed to get a discharge capacity of 1100 mAh/g at 0.1 C. Mumin Rao et al. [12] used a mixture of carbon nanofibers and carbon particles and the same solution-based chemical reaction-deposition method as Ji et al., where the nanofibers were used as electric conductors. They found that adding carbon nanofibers did improve the discharge capacity and the cycling durability. An initial discharge capacity of 1200 mAh/g was reached and a capacity of 668 mAh/g after 50 cycles at 0.05 C. No previous work has been found in which HCNFs were used as conductive matrices or sulfur-host in lithium/sulfur cells.

2.4 Helical Carbon Nanofibers

Helical carbon nanofibers (HCNFs) are carbon nanofibers that are twisted in a helical manner, shown in figure 2.2. They have a diameter of several tens to hundred of nanometers and lengths of a few 100 μm. The HCNFs helical shape makes them a flexible material that potentially do allow for some volumetric flexibility [13]. The possible

flexibility of the material makes the HCNFs a promising material to handle the large volume expansion during discharge in the sulfur containing electrode in lithium/sulfur cells.

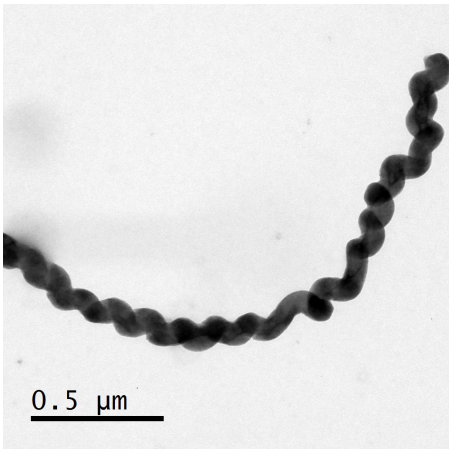

Figure 2.2: TEM image of a helical carbon nanofiber.

2.5 Chemical Vapour Deposition (CVD)

The synthesis of carbon nanostructures and specifically of helical structures are mostly based on different chemical vapor deposition (CVD) techniques. CVD is a technique used to create solid materials by deposition from gas phase with high purity and is commonly used to synthesize different carbon nanostructures. In the CVD process a layer of solid material is deposited on a substrate by chemical reactions between the substrate and the surrounding gases. There exist many different CVD techniques where catalytic CVD is of high interest when creating carbon structures. In catalytic CVD different particles are used as catalysts to synthesize the nanostructures [14]. The catalyst material is often Fe or Ni but other materials can be used as well. The product depends on the catalyst used and the catalyst usually remains in the product after synthesis. Removing the catalyst is difficult, expensive and time consuming but can be done by acid treatment [15]. A more exotic choice are palladium based catalysts that are relatively inert and do not induce magnetic impurities [15]. F. Nitze et. al. did successfully synthesize high purity HCNFs using Pd catalyst at 550 °C in flow of acetylene, ammonia, argon and Varigon (95% argon and 5% hydrogen) [16]. Acetylene acts as a carbon source and ammonia is used as supportive gas that promotes the growth. Synthesizing with only ammonia will not generate high HCNF yield [17]. The addition of hydrogen plays a significant role to grow carbon structures, probably by reducing the oxidized palladium atoms and stimulate the catalyst to produce filament-like structures [18]. Without hydrogen only micro-spheres are synthesized with palladium particles at 800 °C [18]. Argon creates an inert atmosphere and acts as carrier gas.

2.6 Activation of Carbon

Activation of carbon is a process where micropores are formed in the material to increase the surface area. Activation of carbon increases, in general, the porosity, surface area and pore volume [19]. The increased surface area increases the reactivity of the material and activated carbon is thus usually used to filter and remove impurities at low concentrations. Pores smaller than 2 nm are called micropores and pores in the range of 2-50 nm are called mesopores. The main contribution to the surface area originates usually from micropores. The pores within a material do usually differ in sizes and shapes, but their shapes are hard to determine [19].

Two main processes are used to activate carbon, physical and chemical activation. The physical process often uses hot gases to activate carbon. The chemical process uses different chemicals mixed with carbon and heated to a suitable temperature. It has been shown that chemical activation can achieve similar or higher porosity than physical activation. In the case of fibers, chemical activation damages the fibers less [20]. It has further been shown that potassium hydroxide (KOH) generates samples with narrower micropore size distribution than sodium hydroxide (NaOH) [20]. The KOH treatment may be associated with gasification reactions and if the impregnation ratio is low the micropores volume becomes relatively small. Gasification is a process that converts carbon into carbon monoxide, carbon dioxide and hydrogen in high temperature with limited amount of oxygen. It is believed that KOH starts a redox reaction where carbon is initially oxidized to CO or CO_2 which increases the porosity and that K_2CO_3 is formed as a byproduct [21, 22].

2.7 Transmission Electron Microscopy (TEM) and Scanning Electron Microscopy (SEM)

Optical microscopes using visible light can resolve particles down to approximately half of the used wavelength i.e. about 200 nm. This resolution is too small to be able to resolve molecular structures. The resolution limit depends on the wavelength of the used illumination source and thus the wave/particle duality of the electron can be used to resolve even smaller objects due to its small de Broglie wavelength. A 100 keV electron beam can theoretically resolve down to 0.004 nm [23], but this is in reality not possible due to aberration and imperfection in the lens system. Today it is possibel to resolve below 0.5 Å [24] with the most advanced electron microscopes. When using electrons, a lot of secondary signals are formed, for example backscattered, secondary, elastic and inelastic scattered electrons. These signals can be used to obtain additional structural and chemical information besides imaging. The main difference between SEM and TEM is that TEM uses wide-field irradiation of the sample whereas SEM uses scanning irradiation with a focused beam.

In a transmission electron microscope (TEM) the transmitted electrons are used to obtain image information and this means the investigated sample needs to be very thin. The image can be formed by the differences in absorption of the materials within the

sample. Thus the image varies with thickness and density of the material investigated. In high resolution TEM the image is formed from phase contrast due to interference within the electron wave. The incomming electron wave is scattered by the potentials of the atoms within the sample and the phase is changed. The outgoing electron wave holds high resolution information about the sample and that information is magnified by the microscope. The image captured is the interference pattern of the electron waves.

A scanning electron microscope (SEM) is similar to a TEM but analyzes the electrons scattered back from the sample instead of the transmitted ones. This makes it possible to investigate the surface of thicker samples. Usually backscattered electrons and secondary electrons are investigated. Backscattered electrons are electrons elastically scattered by atoms in the specimen. Secondary electrons are electrons that are ejected from atoms in the sample by inelastic scattering from the electron beam, these are often of low energy and contain mostly topological information. Two of the main drawbacks of using electrons instead of light are the risk of local charges in the material and the risk of breakdown of the sample due to intense electron radiation.

2.7.1 Energy-dispersive X-ray Spectroscopy (EDX)

In energy-dispersive X-ray spectroscopy (EDX) a high energy beam of electrons is focused on a sample. The electrons within a material at rest contains ground state electrons quantified in discrete energy shells. If an incoming electron ejects an electron in an inner shell by excitation there will be an electron hole. The hole is filled by an electron from an outer shell and the atom is de-excited. The difference in energy from the outer and the inner shell is released as an X-ray. Since different materials have different electron configurations the elements occuring in the sample can be quantified by measuring the released X-rays.

2.8 Thermogravimetric Analysis (TGA)

Thermogravimetric analysis (TGA) is a method where changes in mass of a sample are measured as a function of increasing temperature or time. The weight losses can usually be correlated to a loss of a specific substance or element, thus the loss can be used to determine the content of that substance or element within the sample. The sulfur content within sulfur-impregnated carbon nanofibers can easily be determined by TGA measurements since sulfur evaporates at much lower temperatures than carbon.

2.9 Brunauer Emmett Teller (BET)

BET is used to measure the surface area and/or porosity of a material. The real name of the technique is actually gas adsorption analysis but BET is usually used as a synonym. In a BET measurement the gas, usually nitrogen, adsorption of a sample is measured as a function of pressure. The adsorbed gas is proportional to the internal and external surface area. A known amount of gas enters the sample and the pressure drops when

the gas is adsorbed. When the pressure reaches it's saturation limit no more adsorption happens despite increased pressure. The sample is then heated and the released nitrogen is measured. This gives the adsorption-desorption curve which is a plot of adsorbed gas versus relative pressure. From the adsorption-desorption curve information about the material surface and pores is revealed.

The BET technique measures the specific surface area by calculating the amount of gas needed to form a single layer on the surfaces. The BET-equation 2.2 tells both the adsorbed volume and the total surface area by using information given by the adsorption-desorption curve [25].

$$\frac{P}{V(P_0 - P)} = \frac{1}{V_m C} + \frac{C-1}{V_m C}\frac{P}{P_0} \tag{2.2}$$

P = Vapour pressure of adsorbate gas at equilibrium and at a certain temperature, P_0 = Saturated vapour pressure, V = Volume of gas adsorbed at the adsorption temperature, V_m = Volume of gas required to fill one monolayer, C = BET-constant. When V_m is determined the total surface area S can be determined by

$$S = \frac{V_m L_{av} A_m}{M_v}. \tag{2.3}$$

At high pressures there is capillary condensation and the pores are filled with liquid. The condensation happens first in the smaller pores. When all the pores are filled, the pressure is decreased and the evaporated gas is measured. The hysteresis between the adsorption and desorption isotherm reveals the size and volume of the pores. The Barrett, Joyner and Halenda theory (BJH) is used to calculate the pore size distribution of a material by using a modified Kelvin equation which is based on cylindrical pores [26]. BJH usually underestimates small pores and does only apply to mesopores and small macropores.

3

Fabrication and Methodology

In this section the construction, assembly and testing of the cells are described. In figure 3.1 a schematic configuration of the coin cells used for battery tests in this thesis is shown. The cell consist of two electrodes, a lithium metal one and a sulfur impregnated HCNFs one. The electrodes are soaked in electrolyte, electrical insulated by a separator and enclosed in a coin cell shell.

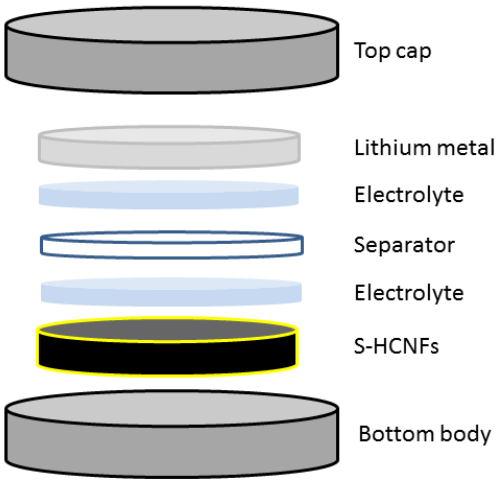

Figure 3.1: Assembly setup of a coin cell

3.1 Synthesis of Helical Carbon Nanofibers

The synthesis method used to produce the HCNFs is similar to the robust synthesis technique described by F. Nitze et al. [16]. HCNFs where synthesized by CVD in a tube furnace, a schematic setup is shown in figure 3.2. The catalyst was prepared by mixing 98 mg tris(dibenzylidenacetone)-dipalladium(0)(Pd_2dba_3) and 77 mg C_{60} dispersed in 1 ml of toluene. The mixture was sonicated for 2 minutes and was then drop casted on a silica wafer at 50 °C. The product was annealed in an oven at 200 °C for 2 hours to remove all ligands (dba). The catalyst wafer was then placed inside a quartz tube in the CVD-system. The sealed system was typically preheated for 20 min in 75 ml/min argon flow to 550 °C, pretreated in 75 ml/min argon, 75 ml/min Varigon (95% argon and 5% hydrogen) and 25 ml/min ammonia and after 20 minutes 20 ml/min of acetylene gas was added for 160 minutes.

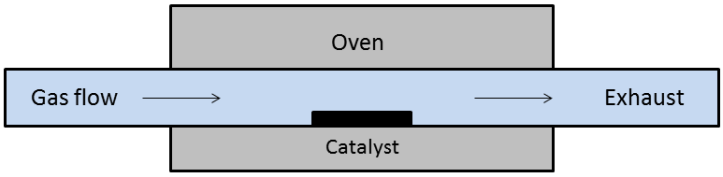

Figure 3.2: Schematic of a CVD setup in which carbon nano-structures are grown.

3.2 Reference Material

Initially straight carbon nanofibers were intended to be used as reference fibers, but due to failed deliveries multi-walled carbon nanotubes (MWCNTs) were used (MRCSDS Catalytic Multi-Wall Carbon Nanotubes, MER Corporation) with diameters about 80 nm. MWCNTs consist of several layers of graphene sheets rolled into cylindrical nanotubes.

3.3 Activation

The activation was done by mixing potassium hydroxide and HCNFs in the ratios 2:1 or 3:1. The former was heated to 750 °C [20] and the second to 800 °C following and adopting the procedures described in reference [3] and [27]. Both mixtures were slowly heated from room temperature for two hours and kept at the corresponding temperature for 60 minutes. The products were then washed in 5 M hydrochloric acid three times to remove the KOH and then filtered in distilled water for at least five times. Filtration and recovery of the product were done by vacuum filtration. The product was then dried at at least 100 °C for at least two hours.

3.4 Cathode Preparation

HCNFs were sulfur impregnated by melt-diffusion. HCNFs and elemental sulfur were mixed in weight ratio 50:50 and heated at 155 °C for two or eight hours. The 8 hour heating time was used in cells tested for 50 cycles and 155 °C is the temperature at which sulfur has its lowest viscosity, facilitating the introduction of sulfur into the pores. The S-HCNFs were then heated to 200 °C for 45 min to remove sulfur on the surface of the S-HCNFs. The cathodes where prepared by mixing 100 mg S-HCNFs, 10 mg polyvinylidene fluoride (PVDF) and 0.75 - 1,5 ml N-methyl-2-pyrrolidone (NMP) or at corresponding ratio to obtain larger amounts of slurry. The mixture was ball milled for 10 minutes at 10 Hz or 30 min at 20 Hz depending on the slurry forming properties of the HCNFs. The activated HCNFs were easier to disperse than the native HCNFs. Thus the activated HCNFs were ball-milled at lower frequency. The slurry was blade casted on a smooth alumina foil by gliding a doctor blade over the slurry. The slurry was then dried in an oven at around 100 °C for 1 hour.

3.5 Characterization

TEM and SEM were used to visualize the structure and the morphology of the different fibers and cathodes. When using TEM the fibers were dispersed in ethanol by ultrasonication and drop casted onto carbon film coated copper TEM-grids. The grids were dried at 60 °C to remove ethanol and investigated in a Tecnai FEI at 200 keV. In the SEM the as prepared cathodes were directly investigated (Ultra 55 FEG SEM Zeiss). EDX analysis was used to investigate the occurring elements and the sulfur distribution within the samples. To investigate the sulfur and palladium content of the samples TGA was used. The palladium content was determined in pure oxygen in an alumina crucible and investigated by heating 10 °C/min from 25 °C to 900 °C (Mettler Toledo TGA/DSC 1 LF/948). For the sulfur content samples were heated in nitrogen gas flow in an aluminum crucible and was investigated by heating in the same rate up to 500 °C followed by isothermal treatment for 30 min (Perkin Elmer TGA 7). BET/BJH were used to check the surface area, porosity and pore distribution of the samples (Micrometrics Tristar 3000).

3.6 Cell assembly and Testing

The cathodes were tested by assembling coin cells using equimolar lithium bis(trifluoromethanesulfonyl)imide (LiTFSI) and tetraethylene glycol dimethyl ether (tetraglyme) as electrolyte, lithium metal as anode and cellgard 2320 as separator as shown in figure 3.1. The circular electrodes had a diameter of 1 cm and the sulfur cathode had a mass of about 0.6-2 mg per cathode, corresponding to a sulfur mass of 0.3-1 mg per cathode or 0.4 - 1.3 mg cm^{-2}. The cells were assembled in an argon-filled glove box. Cycling and rate performance tests were done on a Scribner 580 battery tester system, in the range of 1.5-2.8 V.

The cells were initially tested by cycling 5 times per rate at C/20, C/10, C/5, C/2, C, C, C/2, C/5, C/10 and C/20, where C is defined as the current where the cell would be theoretically discharged in one hour if all sulfur was utilized. Subsequently some cells were cycled 50 times at C/10 to further investigate the cyclability.

4

Results and Discussion

4.1 Synthesis of Helical Carbon Nanofibers

TEM images of HCNFs synthesized as described in the fabrication and methodology part are shown in figure 4.1. The synthesized fibers are helically shaped, have diameters between 50 and 100 nm and length in the range of several micrometers. The dark triangle inside the black circle in figure 4.1(a) is a palladium catalyst particle. The palladium particles remain from the synthesis and are enclosed inside the HCNFs. The shown fibers are of high quality, but there are some impurities present in the samples due to not optimal synthesis conditions. The resulting batches varied considerably in yield and quality, this could have been due to degraded Pd_2dba_3 or use of too little solvent in the catalyst preparation phase. After initial CVD synthesis some attempts to increase the yield were done by adding small amounts of water during syntheses. This did unfortunately reduce the yield and purity of the HCNFs in contradiction to the earlier reported synthesis approach [16]. The initial conditions where used for the rest of the syntheses. It is however not unusual that CVD batches vary due to small changes in the CVD setup. The batches with the highest purity where used to prepare cathodes. In figure 4.1(c) sulfur impregnated not activated HCNFs (S-HCNFs) at ratio 50:50 are shown. The HCNFs with and without sulfur look the same so it is not possible to tell whether the sulfur is on the surface of the HCNFs, inside the pores or in chunks somewhere else by investigating the TEM images. This can most certainly be attributed to the low mass difference between sulfur and carbon resulting in very low contrast between the two elements.

4.2 Activated Fibers

HCNFs activated with potassium hydroxide (KOH) in the mass ratio 2:1 (twice as much KOH as HCNFs) are shown in figure 4.2(a) and 4.2(b). The fibers are still helical,

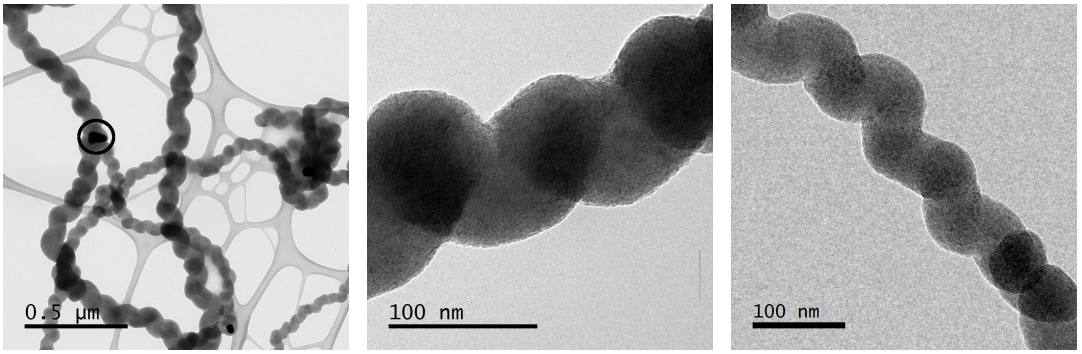

(a) HCNFs (b) HCNFs (c) Sulfur impregnated HCNFs 50:50

Figure 4.1: TEM images of HCNFs and S-HCNFs. (a) and (b) show pristine HCNFs where the circle in (a) indicates a palldium particle. (c) shows a sulfur impregnated HCNF in ratio 50:50.

maybe somewhat damaged but the overall morphology has only slightly changed. The activated fibers are visually very similar to the pristine HCNFs. The activated HCNFs 2:1 impregnated with sulfur 50:50 are shown in 4.2(c), the sulfur is hard to distinguish from the carbon as concluded in the previous section.

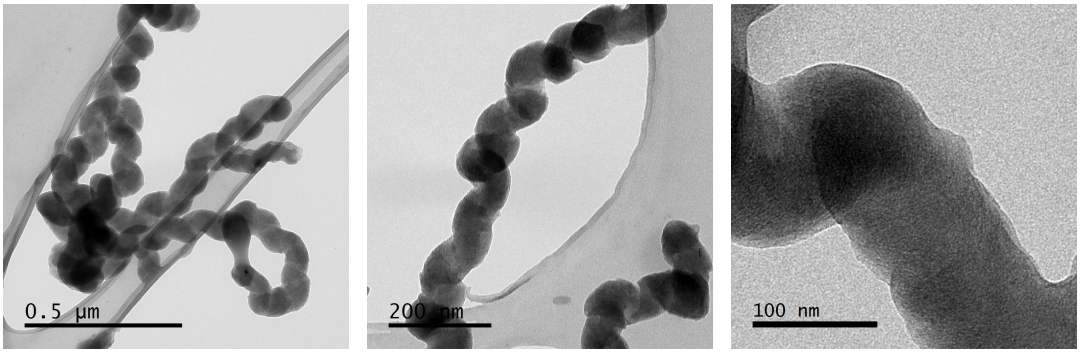

(a) Activated HCNFs 2:1 (b) Activated HCNFs 2:1 (c) Activated HCNFs 2:1, sulfur impregnated 50:50

Figure 4.2: TEM images of activated HCNFs 2:1 (a-b) and corresponding fibers sulfur impregnated 50:50 (c).

HCNFs activated in the ratio of 3:1 are shown in figure 4.3(a) and 4.3(b). They are still intact and helically shaped and are also visually very similar to the pristine HCNFs. In figure 4.3(b) there are some darker spots, indicating the occurrence of some regions with higher density or stronger scattering properties than carbon. This might be residues of K_2CO_3 formed in the activation process [22].

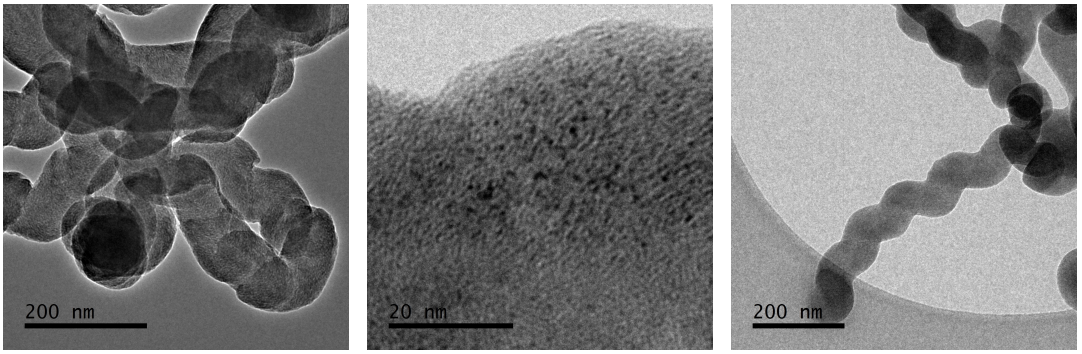

(a) Activated HCNFs 3:1 (b) Activated HCNFs 3:1 (c) Activated 3:1 HCNFs, sulfur impregnated 50:50

Figure 4.3: TEM images of activated HCNFs 3:1 (a-b) and corresponding fibers sulfur impregnated 50:50 (c).

4.3 Reference Material

TEM images of the materials for the reference cells (MWCNTs) are shown in figure 4.4. They have a straight structure with diameters around 80 nm and lengths of several micrometers (For an overview image see section 4.4 Cathodes). In figure 4.4(a) the highly ordered structure of the carbon nanotubes wall is shown together with a thin amorphous region close to the surface of the fiber. In figure 4.4(b) an activated MWCNT 2:1 is shown. It has a less ordered atomic structure than the pristine MWCNT, indicating that the activation introduces pores in the tubes. In figure 4.4(c) the over-all structure of the activated tubes is shown.

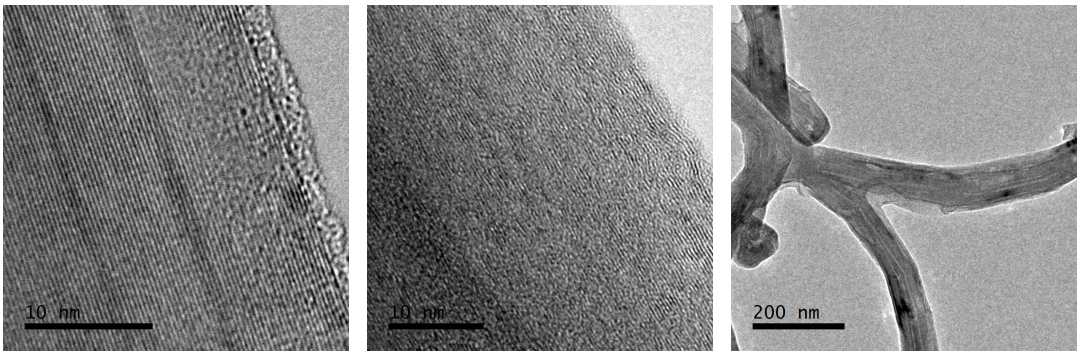

(a) MWCNTs (b) MWCNTs activated 2:1 (c) MWCNTs activated 2:1

Figure 4.4: The used reference material consisting of MWCNTs (a). Activated MWCNTs 2:1 are shown in (b) and (c).

Sulfur impregnated MWCNTs and sulfur impregnated activated MWCNTs are shown in figure 4.5. In figure 4.5(a) and 4.5(b) sulfur impregnated MWCNTs are shown, where in the later an outer more amorphous region is visible. This region might be attributed to a mixture of sulfur and amorphous carbon covering the tube, or only amorphouse carbon as in the pristine case. In figure 4.5(c) activated sulfur impregnated MWCNTs are shown.

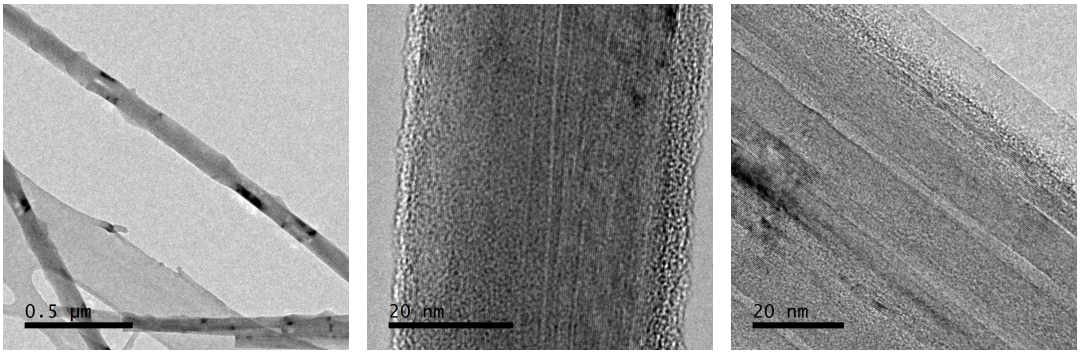

(a) MWCNTs sulfur impregnated 50:50

(b) MWCNTs sulfur impregnated 50:50

(c) MWCNTs activated 2:1 sulfur impregnated 50:50

Figure 4.5: Sulfur impregnated MWCNTs are shown in (a) and (b). Activated sulfur impregnated MWCNTs are shown in (c).

4.4 Cathodes

SEM images of cathodes consisting of sulfur impregnated HCNFs 50:50 mixed with 10 % PVDF binder are shown in figure 4.6. The S-HCNFs form a homogenous film with the PVDF binder and no heterogeneous regions can be found indicating a good distribution of sulfur. The coating is even over the aluminum foil, indicating that a good dispersion of the slurry was achieved. If assessing the cathodes from these images it is reasonable to believe that the cathode should easily manage volume expansions and contractions due to the entanglement and helicity of the HCNFs. Equal cathodes but with HCNFs activated 2:1 and 3:1 are shown in 4.7 and 4.8, respectively. The activated fibers are visually almost equal to the non activated HCNFs except some minor damages, as concluded in the TEM images. They are still entangled as shown in figure 4.8(b).

Due to difficulties to form a nice slurry the coating uniformity varied between the cathodes and even within single cathodes. In figure 4.6 the fibers are nicely uniformly coated on the aluminum foil, but in figure 4.7(b) and 4.8(a) the aluminum foil is exposed in the background. In figure 4.7(a) a part with a dark cloud is shown, this is probably the PVDF binder that is not uniformly dispersed. In all of the cathodes there are mainly HCNFs, but some impurities of other carbon structures exists in a mixture with the HCNFs. The impurities are probably not a major issue, as long as they are relatively

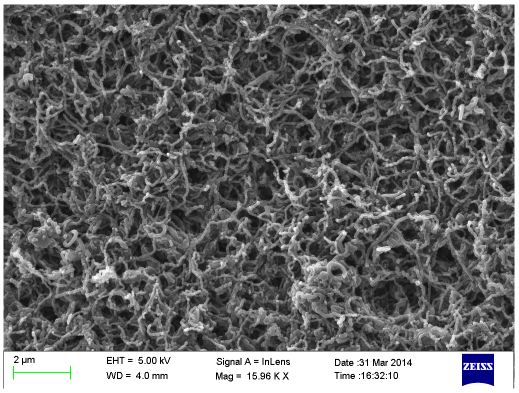

(a) Sulfur impregnated HCNFs (Scale bar: 2 μm)

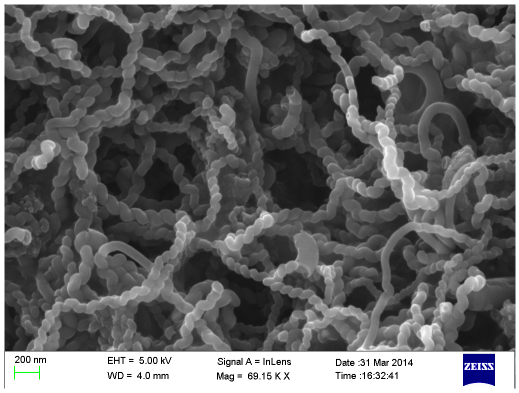

(b) Sulfur impregnated HCNFs (Scale bar: 0.2 μm)

Figure 4.6: SEM images of a cathode containing sulfur impregnated HCNFs mixed with 10 % PVDF binder.

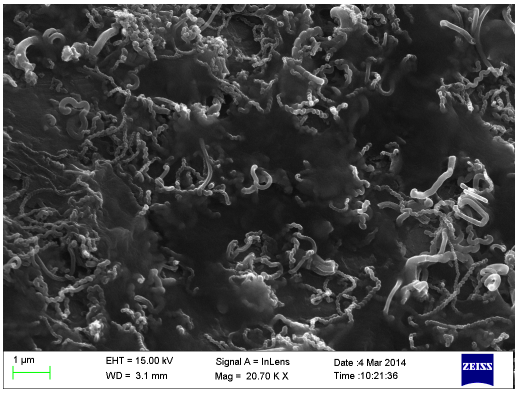

(a) Sulfur impregnated activated HCNFs 2:1 (Scale bar: 1 μm)

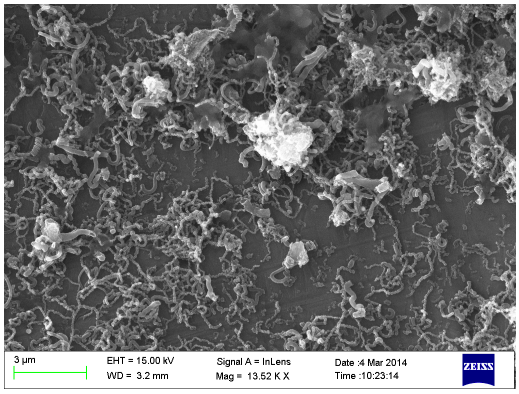

(b) Sulfur impregnated activated HCNFs 2:1 (Scale bar: 3 μm)

Figure 4.7: SEM images of a cathode containing sulfur impregnated activated HCNFs 2:1 mixed with 10 % PVDF binder.

few, since they are carbon structures and thus well conducting and have similar properties as the HCNFs.

The reference cathodes (MWCNTs) treated and sulfur impregnated in the same way as the HCNFs are shown in figure 4.9. They are fairly evenly coated on the aluminum foil and somewhat entangled. There are mostly MWCNTs in the cathode, but a bigger lump is shown in figure 4.9(b). That is probably sulfur that is not completely evenly distributed throughout the sample. Around some of the fibers there are some kind of adhesive, that might also be sulfur but is probably the PVDF binder. The almost straight structure of the tubes with lengths of a few μm is visible.

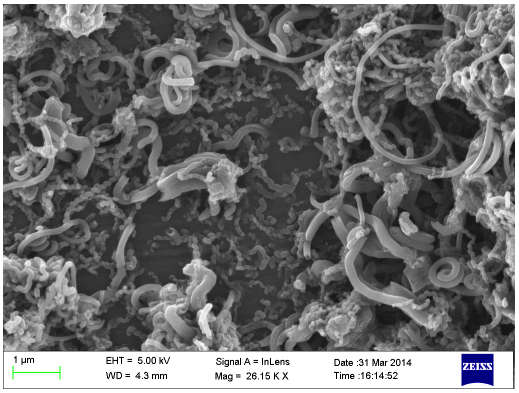

(a) Sulfur impregnated activated HCNFs 3:1 (Scale bar: 1 μm)

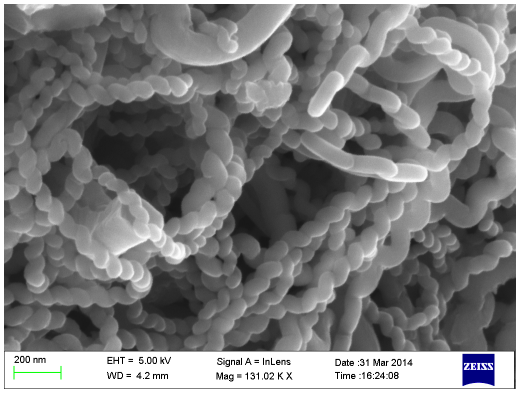

(b) Sulfur impregnated activated HCNFs 3:1 (Scale bar: 0.2 μm)

Figure 4.8: SEM images of a cathode containing sulfur impregnated activated HCNFs 3:1 with 10 % PVDF binder.

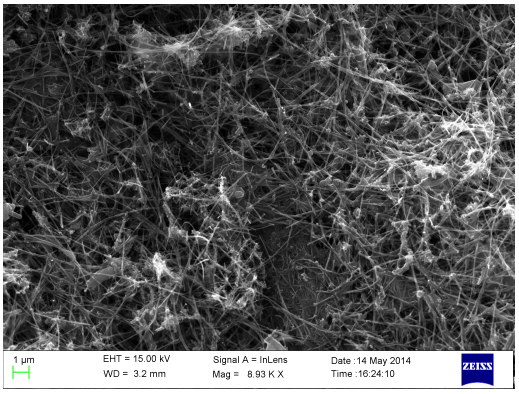

(a) S-MWCNTs cathode (Scale bar: 1 μm)

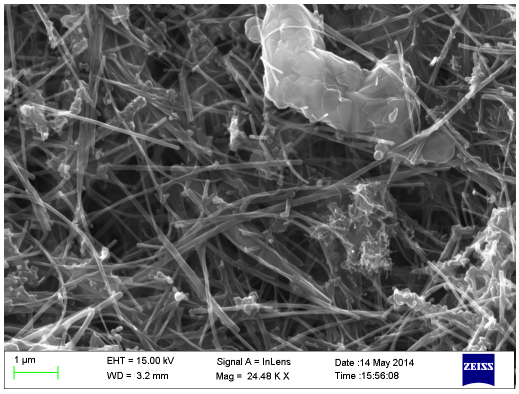

(b) S-MWCNTs cathode (Scale bar: 1 μm)

Figure 4.9: SEM of S-MWCNTs with PVDF

In figure 4.10 the activated MWCNTs 2:1 cathode is shown. From the SEM images the activated tubes look very similar to the non activated MWCNTs.

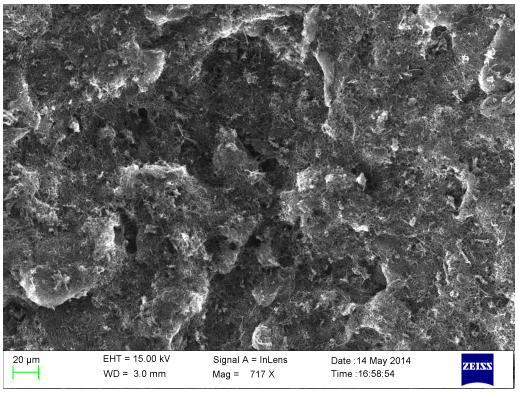

(a) Activated S-MWCNTs 2:1 cathode (Scale bar: 20 μm)

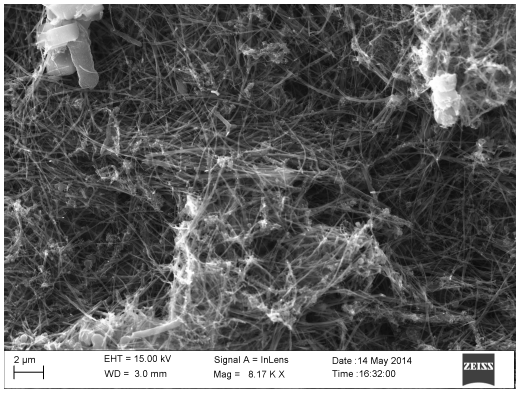

(b) Activated S-MWCNTs 2:1 cathode (Scale bar: 2 μm)

Figure 4.10: SEM of Activated S-MWCNTs 2:1 with PVDF

4.4.1 Cathode preparation - acquired experience

Since dispersing of the fibers was challenging several different preparation methods were tested. In table 4.1 the effects on the slurry forming properties of several factors are shown. The influence of the different factors were mainly tested on pristine HCNFs. In general more violent ball milling is favourable but might at the same time destroy the micro structure of the fibers. Increased amount of solvent also improves the dispersion. But if too much solvent is added the blade coating process becomes complicated and the electrodes usually become thin.

Substance	Affect	Comment
Increased ball-milling freq.	+	Be careful to not destroy the fibers
Increased ball-milling time	+	Be careful to not destroy the fibers
Increased ball size	+	Be careful to not destroy the fibers
Sonication	-	Similar affect as ball-milling but slower
Clean Al-foil with NMP	0	No difference from ethanol
Ethanol as solvent	0	Maybe worse, did at least not improve
PEO as binder	0	No noticed difference
Increased solvent (NMP)	+	To much hamper coating
Activated HCNFs instead of raw	+	
MWCNTs insted of HCNFs	-	

Table 4.1: Tested factors affecting dispersion of fibers.

4.5 Analysis

In this section the HCNFs are carefully analyzed to get a deeper understanding of their atomic spacing, porosity, sulfur content, sulfur distribution and purity of the fibers.

4.5.1 Spacing of Carbon Sheets

The HCNFs consist of graphite sheets predominantly oriented perpendicular to the growth direction, the carbon structure can be seen in figure 4.11 where a HCNF activated 3:1 is shown.

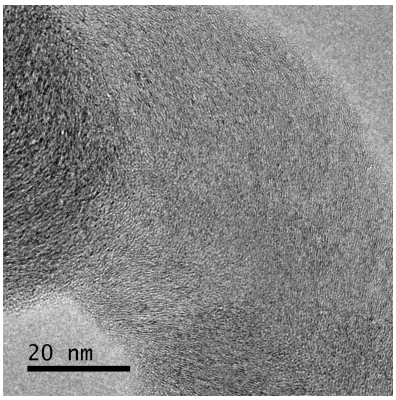

Figure 4.11: HCNF 3:1, carbon spacing

In the TEM images in figure 4.12 the surfaces of the fibers are shown at high magnification. The carbon lattices of the HCNFs are visible. The spacing of carbon sheets appears to be in general similar both before the activation (figure 4.12(a)), after activation 2:1 (figure 4.12(b)) and after activation 3:1. S. Yoon et al. [27] have suggested that the graphene layers become more randomly ordered during activation, which might be observed by comparing the pictures. It is not obvious but the variations between sharp and less sharp carbon lattice areas in figure 4.12(c) might indicate that there are different regions with more and less amorphous carbons. The variations might also be due to pores formed close to or on the surface of the fibers.

S. Yoon et al. also suggest that the interspacing is increased between structures consisting of several sheets. To investigate the interspacing fast fourier transforms (FFT) were performed on the images of the different fibers. In figure 4.13 a FFT of the image with activated HCNFs 2:1 from figure 4.12(b) is shown. The FFT reveals information about the spacing between carbon sheets, However the suggested increased interspacing could not be verified by these TEM pictures.

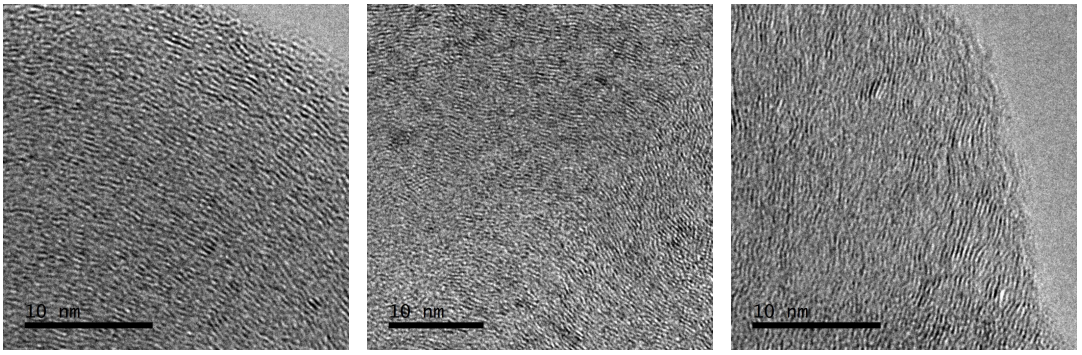

(a) Raw HCNFs (b) Activated HCNFs 2:1 (c) Activated HCNFs 3:1

Figure 4.12: Comparison of carbon spacing between pristine HCNFs, activated HCNFs 2:1 and 3:1.

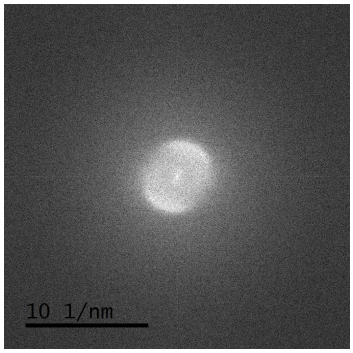

Figure 4.13: FFT of a TEM image of the activated HCNFs 2:1 shown in figure 4.12(b).

4.5.2 Occurring Elements and Distributions

EDX analysis of occurring elements in the sulfur impregnated HCNFs activated 2:1 and 3:1 is shown in table 4.2. The most commonly occurring elements are of course carbon and sulfur from the HCNFs and sulfur impregnation. Other detected elements are palladium, aluminum, fluorine and potassium. The palladium originates from the catalyst particles, the potassium is a residue from the activation process, the fluorine is connected to the PVDF binder and the aluminum is a background from the aluminum foil. The quantification of the elements is probably not entirely correct for the 2:1 HCNFs since equal amounts sulfur and HCNFs were used in the impregnation process. The quantification of elements in the 3:1 case seems more consistent with the TGA measurements. One of the main reasons for this is probably that EDX probes a tear like volume under the surface which in our case might not represent the overall situation.

In figure 4.14(a) a SEM image of the HCNFs activated 2:1 sulfur impregnated 50:50 is shown. The corresponding carbon and sulfur distributions from EDX analysis are shown in figure 4.14(b) and 4.14(c) respectively. Figure 4.14(c) show that the sulfur is

distributed everywhere in and/or around the HCNFs within the limited resolution of the method.

Substance	2:1	3:1
C	64.0	50.0
S	25.9	45.5
Al	3.9	-
F	2.8	-
Pd	2.8	3.7
K	0.7	0.8

Table 4.2: Weight% of occurring elements in HCNFs activated at ratios 2:1 and 3:1 from EDX-analysis.

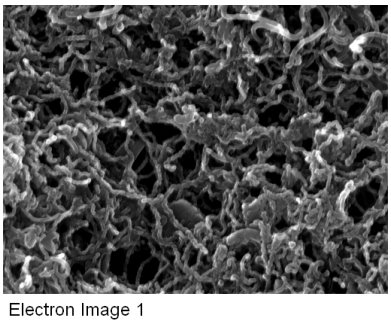

(a) Sulfur impregnated HCNFs 50:50

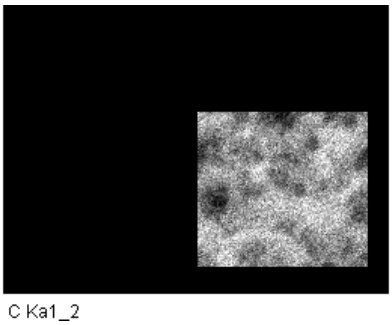

(b) Carbon distribution of figure 4.14(a))

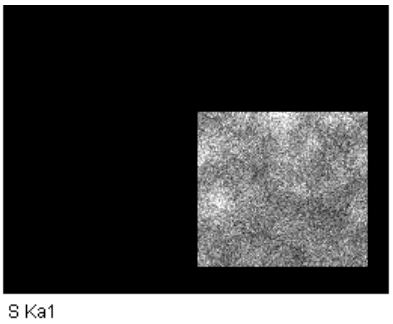

(c) Sulfur distribution of figure 4.14(a)

Figure 4.14: Distribution of carbon and sulfur in sulfur impregnated HCNFs 50:50 from SEM/EDX analysis.

4.5.3 Porosity

The adsorption-desorption curves and BJH pore distributions of HCNFs and MWCNTs are shown in figure 4.15(a) and 4.15(b), respectively. The HCNFs have some porosity already before activation. The activation process significantly increases the porosity in the mesoporous range as shown in the graph, which is consistent with the results of Deng et al. [3]. After sulfur impregnation for 2 hours the porosity is significantly decreased. This indicates that the pores are filled (or at least completely clogged) with sulfur. Worth remembering is that the BJH method is not fully reliable in the low mesoporous range but it still gives an indication that the porosity is significantly increased by activation with KOH. The BET surface areas and the total BJH pore volumes are shown in table 4.3. In general the pore volume and surface area are significantly increased by activation and significantly decreased by sulfur impregnation. Increased pore volume and area is a clear sign of significantly increased porosity. The decreased surface area due to sulfur impregnation indicates that the small mesopores/micropores are filled with sulfur. In contradiction to the results of Deng et al. the sulfur impregnated HCNFs have lower porosity than the pristine HCNFs, but that is probably because Deng et. al. used a lower fraction of sulfur. The activated MWCNTs are less porous than the activated HCNFs, MWCNTs are known to be more inert and require therefore probably higher activation ratio, temperature or time to reach corresponding porosity as the HCNFs. The HCNFs mean pore size decreases after activation which indicates that the activation process forms new pores, smaller than the existing. But in the MWCNTs the pore size is increased which might be due to less formation of new pores and instead an increase in volume of the already existing ones. If this is the case it might not be possible to activate the MWCNTs to the same extent as the HCNFs.

If the weight of sulfur is approximately 2 g/cm^3 and the porosity of the activated HCNFs is 0.33 cm^3/g the weight fraction of sulfur that can be stored in the pores should be around 40%.

Sample	BET surface area (m^2/g)	BJH pore volume (cm^3/g)	BJH pore size (nm)
HCNFs	39.4	0.09	10.9
HCNFs 2:1	467.7	0.26	7.8
HCNFs 3:1	596.1	0.33	5.1
S-HCNFs 2:1	10.1	0.06	27.2
MWCNTs	28.8	0.09	10.0
MWCNTs 2:1	50.2	0.15	10.8
S-MWCNTs 2:1	13.2	0.05	16.4

Table 4.3: Surface area and porosity of different fibers.

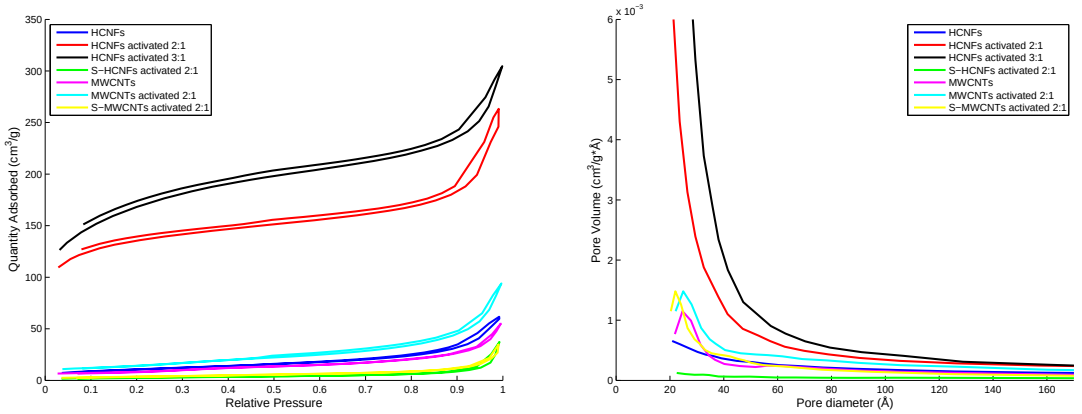

(a) Adsorption desorption curve

(b) BJH pore size distribution

Figure 4.15: Absorption-desorption curves (a) and BJH pore size distributions (b) from several differently treated fibers and tubes.

4.5.4 Sulfur and Palladium Contents

TGA is used to determine the sulfur and palladium content of the samples. In figure 4.16 the results from the TGA measurements are shown. Measurements of HCNFs are shown in figure 4.16(a) and of MWCNTs are shown in figure 4.16(b). The weight decrease of the sulfur impregnated fibers is related to the sublimation of sulfur since the fibers without sulfur do not significantly decrease in weight. All the sulfur impregnated fibers show a sulfur content of 47-50%. During heating the activated (and sulfur containing) HCNFs do not decrease in mass as fast as the non activated HCNFs. This may be due to the higher porosity of the activated fibers and thus higher proportion of sulfur impregnated into the activated HCNFs. Sulfur in pores do probably evaporate slower than free sulfur, or sulfur on the surface, due to capillary forces similar to the hysteresis in BET. The sulfur in the HCNFs activated 3:1 sublimates the slowest which may indicate that these enclose sulfur the most inside the pores, which is reasonable since they have the highest porosity. The slower evaporation of sulfur in pores is confirmed with TGA measurements performed on mesoporous carbon with similar porosity [28].

The small loss in weight of the HCNFs activated 2:1 is most probably evaporation of water. They were simply not sufficiently dried or absorbed water before the TGA analysis. Another possible reason of the decrease could be that some KOH is left in the fibers and thus the activation is continued upon heating. The S-HCNFs 2:1 curve is added to the MWCNTs plot for comparison to show that the sulfur is evaporated much faster in the activated MWCNTs than in the activated HCNFs. The evaporation of sulfur in the MWCNTs and activated MWCNTs are very similar to the evaporation in the non activated HCNFs.

TGA analysis of HCNFs without sulfur is shown in figure 4.17, where 4.17(b) is a

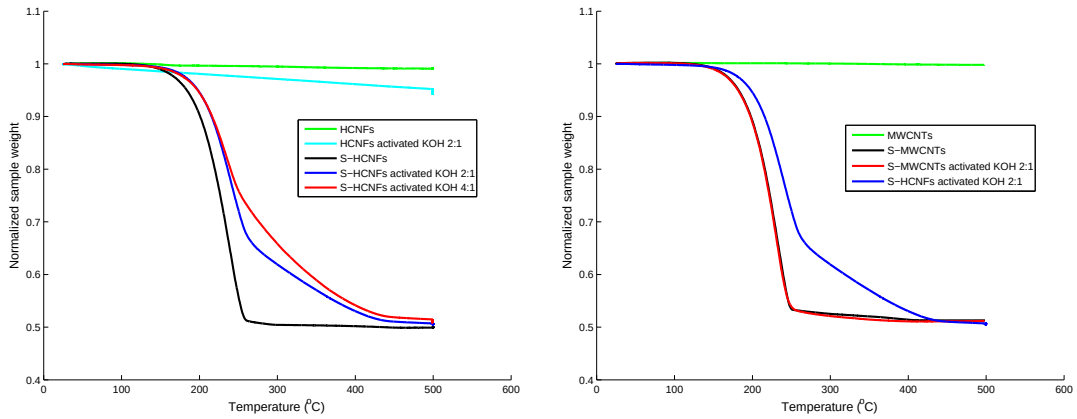

(a) HCNFs (b) MWCNTs

Figure 4.16: Thermogravimetric analysis of HCNFs and MWCNTs to determine sulfur contents.

zoom in of the high temeperature region of figure 4.17(a). The temperature range is increased and the measurements are performed in air. The mass decrease in this case is due to oxidation of carbon and possibly other residues. Palladium oxide is formed since the fibers are burned in air at high temperature, but palladium oxide does decompose to palladium metal above 814 $°C$ [29]. The weight loss due to palladium oxide reverted to palladium metal is shown in figure 4.17(b) at around 800 $°C$. The weight losses due to released oxygen should be 13 wt% [29]. By defining that slope to be 13 % the palladium oxide contents of the HCNFs and the activated HCNFs 2:1 are determined to 3.6 % and 3.9 %, respectively, corresponding to palladium contents within the fibers of 3.2 % and 3.4 %. Since the palladium content (actual weight in graph at 900 $°C$) in the raw data of the HCNFs was initially around 1 % the curve has been adjusted by an increase of 2.2 % to match the correct palladium content. The initial mismatch might have been due to faulty weighing of sample when starting the measurement, or poorly done reference measurement with empty crucible. The calculated palladium content does approximately fit the yield from the CVD synthesis.

The calculated palladium content of the activated HCNFs did however match the total weight at 900 $°C$. The palladium content in these fibers is somewhat higher than the pristine HCNFs, that is related to that some carbon is etched away during activation which increases the fraction of palladium within the fibers. The mass loss at temperatures lower than 500 $°C$ is higher for the activated fibers indicating easier oxidation or evaporation of water that remains from the cleaning after the activation process.

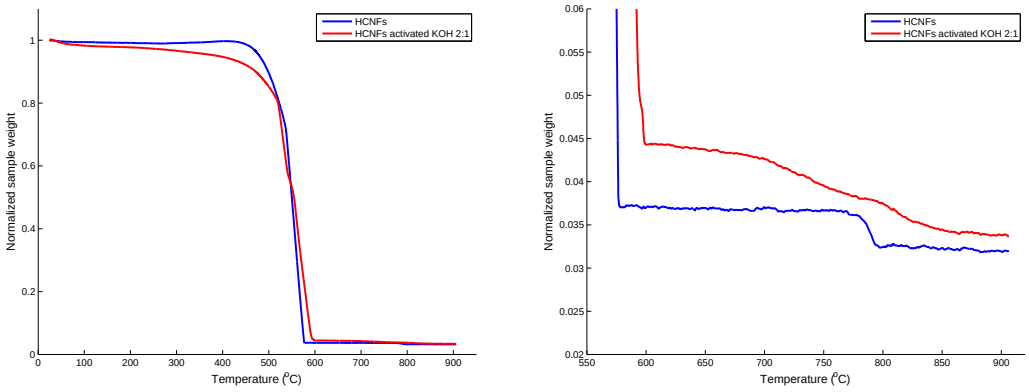

(a) (b)

Figure 4.17: TGA analysis of palladium content in HCNFs.

4.6 Cycling Tests

To be able to tell if the HCNFs are a potential material for lithium/sulfur batteries and if they reduce the impact of the volume expansion/contraction during discharge/charge, cycling tests were performed. Cycling with different C-rates were initially done to see how different charge/discharge rates affected the performance. Subsequently 50 cycles were run to see the performance of the HCNFs over a larger amounts of cycles. CV-cycling was also performed to determine the electrochemical characteristics of the material. All of the specific capacities are calculated by the weight of sulfur in the cathodes and all of the cathodes consists of approximately 45 wt% sulfur. 1 C is defined as the current at which the cell is theoretically discharged in one hour.

4.6.1 C-rate Cycling

C-rate cyclings were performed and the raw data from an experiment is shown in figure 4.18 where HCNFs activated 3:1 are tested. The potential is measured as a function of time during a fixed discharge/charge current. The first five peaks correspond to a discharge/charge current at C/20, then the discharge/charge rate was changed every fifth cycle to C/10, C/5, C/2, C and back up to C/20 again.

The specific discharge capacity of each of those cycles are shown in figure 4.19. In general the specific capacity for the fibers increases with decreased discharge rate and the activated fibers do utilize the sulfur better than the pristine fibers which is in agreement with most studies in literature [3, 11]. At low discharge rates (C/20, C/10) the activated HCNFs have almost twice as high specific capacity as the MWCNTs, while the pristine HCNFs have slightly lower specific capacity than the MWCNTs. The activation of the HCNFs does clearly improve the discharge capacity but does not affect the MWCNTs in the same extent. The improved capacity by activation is most likely related to a larger

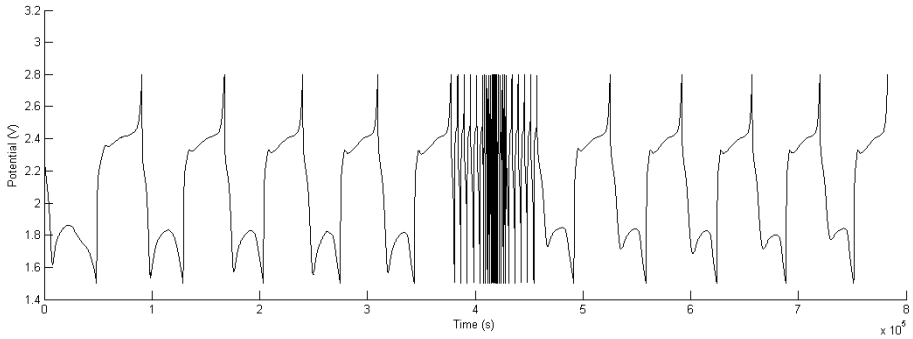

Figure 4.18: Example of raw data from a C-rate cycling experiment.

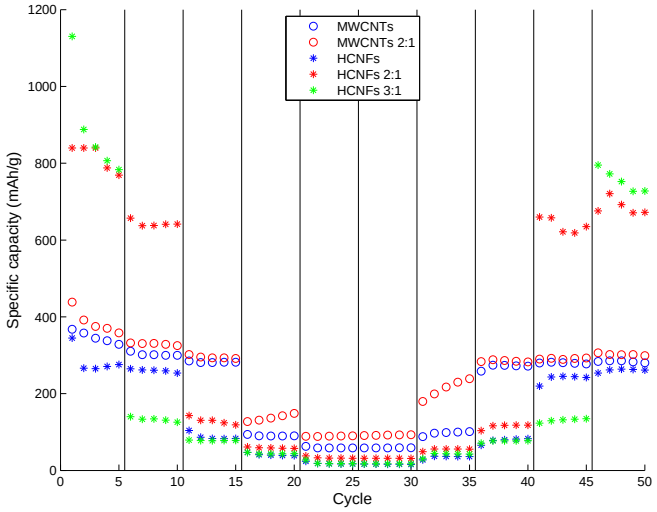

Figure 4.19: Specific capacity for each cycle at C-rate cycling.

amount of sulfur in small mesopores/micropores in the HCNFs and thus better contact between sulfur and the conducting HCNFs. With better contact the utilization of the sulfur is increased. Even higher activation could maybe increase the capacity, but at the same time it would probably further reduce the conductivity and thus further decrease the highest discharge rate that can be used. The MWCNTs are less porous and it is unknown whether increased activation of the MWCNTs to a degree corresponding to the HCNFs would give equal capacity. At high discharge rates (C/5, C/2, C) the MWCNTs have better capacity than the HCNFs. This is probably due to a higher conductivity. The large drop in capacity at C/10 of the activated HCNFs 3:1 is due to that the valley before the hump at C/20 in figure 4.18 gets deeper at higher discharge rates due to not high enough conductivity. The potential falls below 1.5 V before the hump starts and thus capacity is lost or more precisely, not measured. This can be shown by cyclic

voltammetry, see the cyclic voltammetry section.

In most references where activated carbon fibers are used, discharge rates above C/5 are rarely investigated [3, 10, 11]. The problem with low specific capacity at high discharge rates is thus presumably a common problem for lithium/sulfur cells using activated carbon nanofibers.

In figure 4.20 the last cycle in the C-rate cycling is shown for the different materials. The cells are first discharged and then charged, the discharge profiles are easily observed. The HCNFs activated 2:1 do have a potential plateau just below 2 V, while the plateau for the HCNFs activated 3:1 is around 1.8. This is probably due to decreased conductivity in the more activated fibers.

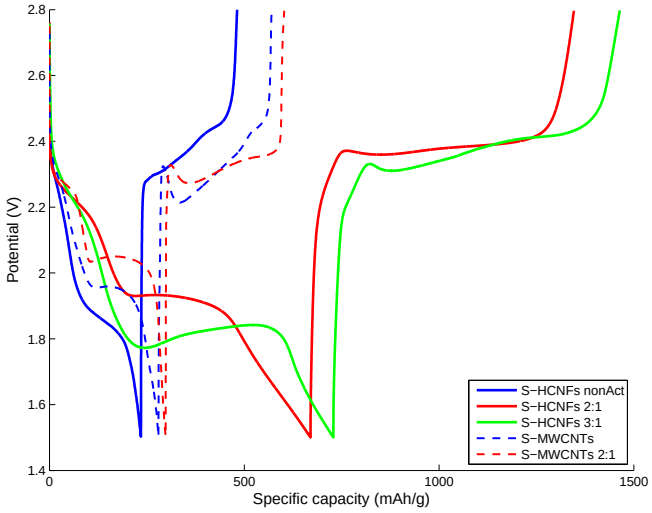

Figure 4.20: The 50th cycles after C-rate cycling. Discharge at C/20.

4.6.2 50 Cycles

Specific discharge capacity of HCNFs and MWCNTs both activated 2:1 and annealed with equal amounts of sulfur/fibers for 8 hours are shown in figure 4.21(a). They are cycled 50 times at C/10. The HCNFs have an initial capacity of 1114 mAh/g but decreases quickly to less than 800 mAh/g. After 50 cycles the HCNFs do remain at a specific capacity of more than 560 mAh/g. The MWCNTs have an initial capacity of 483 mAh/g and remain above 330 mAh/g after 50 cycles. The specific capacity of the HCNFs is significantly higher than for the MWCNTs over 50 cycles but the capacity loss per cycle is larger.

The relative specific capacity is shown in figure 4.21(b), where the initial specific capacities are normalized to one. The HCNFs fade in capacity slightly faster than the MWCNTs. The lower specific capacity in the MWCNTs might favour their cycle

stability. To further evaluate the HCNFs cyclability, straight carbon nanofibers with equal specific capacity are desirable.

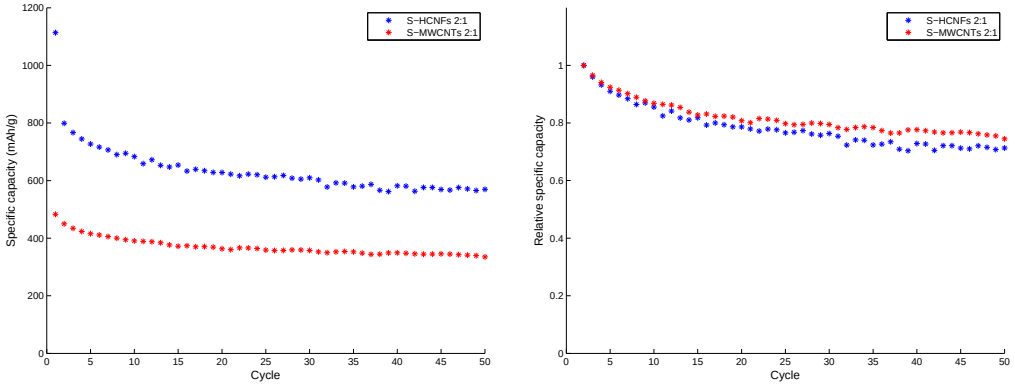

(a) Specific capacity

(b) Relative specific capacity

Figure 4.21: Specific capacity (a) and relative specific capacity (b) of S-HCNFs and S-MWCNTs cycled 50 times at C/10.

The coulombic efficiency for each cycle is shown in figure 4.22. The coluombic efficiency is the discharge capacity divided by the charge capacity. The efficiency is above 95 % for both of the fibers, but is highest for the MWCNTs. Between cycle 20 and 50 the HCNFs and MWCNTs have a mean coulombic efficiency of 97.0% and 99.3 %, respectively. The coulombic efficiency is usually decreased by unwanted side reactions, so the lower coulombic efficiency might be due to a larger shuttle effect and self-discharge. The initial efficiency is higher than one due to cells assembled in their charged states. Even if the efficiency of the HCNFs is worse than for the MWCNTs it is still higher than the results of Z. Deng et al. where they used straight nano fibers activated under almost the same conditions as used in this work [3]. Z. Deng et al. obtained similar specific capacity per mass elemental sulfur and still used less sulfur loading in the cathode. However, the results are overall very similar.

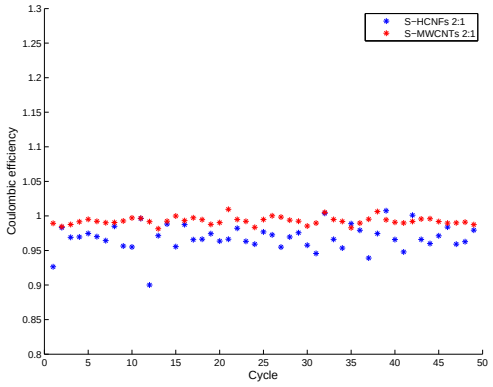

Figure 4.22: Coulombic efficiency

4.6.3 Cyclic Voltammetry

Cyclic voltammetry (CV) of a cycled S-HCNFs activated 2:1 cell is shown in figure 4.23. The cell was cycled with a voltage scan rate of 0.0001 V/s. There are two pronounced discharge peaks at 2.2 V and 1.5 V. The first reduction peak at 2.2 V is due to elemental sulfur reduced into lithium polysulfides (Li_2S_{4-8}) and the second peak around 1.5 V is related the formation of the polysulfides Li_2S_2 and Li_2S [30]. The reduction peaks are usually around 1.9 V and 2.3 V for carbon nanofibers [3, 11, 31] and carbon nanotubes [32]. So the peak at 1.5 V is low in voltage compared to the literature. Since [3, 11, 31] uses carbon black within their cathodes the low voltage peak is likely due to conductivity issues. The cycling tests are limited to voltages above 1.5 V. Since the peak stretches also below 1.5 V, the specific capacity can be increased in the measurements by increasing the discharge voltage range. At high discharge rates the 1.5 V peak is probably shifted to lower voltages, which means that it shifts outside the measurement boundaries.

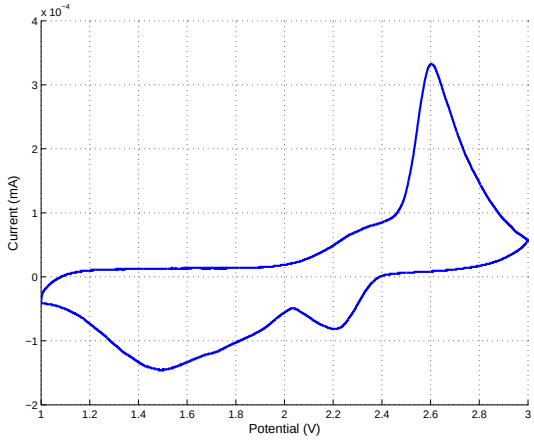

Figure 4.23: Cyclic voltammetry of sulfur impregnated HCNFs activated 2:1

5

Conclusion

In this thesis helical carbon nanofibers (HCNFs) were synthesized and investigated as potential cathode material in lithium-sulfur batteries. HCNFs were thought to be a great material that potentially can withstand the volume increase/decrease during discharge/charge by "breathing". It has successfully been shown that HCNFs can be used as sulfur host in Li-S batteries.

The HCNFs were synthesized by chemical vapor deposition with palladium particles as catalysts. They have diameters between 50 and 100 nm, lengths of several micrometers and palladium content around wt3.3 %. The HCNFs were activated by potassium hydroxide to increase the porosity and the surface area. The porosity was increased from 0.09 cm^3/g to 0.33 cm^3/g to be able to impregnate more sulfur into the pores. The activation might have increased the disorder in the orientation of the graphite sheets in the HCNFs. Multi-walled carbon nanotubes treated in the same way as the HCNFs were used as reference

To create cathodes, the HCNFs were mixed with equal amounts of sulfur and annealed followed by mixing with 10 % PVDF binder and coated onto alumina foil. The sulfur was uniformly distributed within the cathode and the fibers had sulfur contents of around 47-50 wt%. TGA could show that sulfur in activated HCNFs did evaporate slower than in pristine HCNFs which is believed to be due to the increased porosity and better trapping inside small pores. The cathodes were used in coin cells to investigate their cyclability and electric properties at different discharge rates. The activated HCNFs did show great specific capacity at low discharge rates, almost twice as high as for MWCNTs. At higher discharge rates the specific capacity is significantly decreased. This is probably due to insufficient electric conductivity. To investigate the cyclability 50 charge/discharge cycles were performed. The HCNFs retained a discharge capacity of more than 560 mAh/g over 50 cycles with a coulombic efficiency of 97.0%.

5.1 Outlook

The activated HCNFs do show high potential in the performed tests. But it is still not possible to clearly judge if the cyclability is improved without comparing with straight nanofibers and thus tests with straight nanofibers at equal conditions should be done. Since the cathodes tested only have thicknesses of a few micrometers it is unknown whether the ability to expand/contract is extensively tested. Thicker cathodes should be investigated to further investigate the breathing properties and to see if cracks are avoided. To check the cyclability of the cathodes used, already cycled cathodes could be investigated by SEM to look for cracks.

Another related problem is the capacity fade at higher discharge rates that must be tackled. This might be done by adding carbon black or some other highly conducting additive. To further increase the specific capacity even higher porosity is desired, a higher amount of KOH or higher temperature could be used for the activation process. But at the same time, higher activation seems to decrease the conductivity. To further increase the specific capacity further investigations should be performed aiming at both increasing the conductivity and the porosity of the HCNFs. Different kinds of carbon-carbon composites could be investigated, such as mixing small amounts of MWCNTs with HCNFs to increase the conductivity while keeping a high specific capacity. The MWCNTs could act as conducting highways while the HCNFs would act as sulfur hosts. Increased lengths of the HCNFs might also increase the makroscopic electrode conductivity, but might be difficult to synthesis.

To further understand the electrochemical properties of the cathodes complete CV tests should be done with activated and pristine HCNFs, cycled and not cycled. Also resistivity measurements could be interesting.

Bibliography

[1] R. Huggins, Advanced Batteries, Springer.

[2] Liquid electrolyte lithium/sulfur battery: Fundamental chemistry, problems, and solutions, Journal of Power Sources 231 (0) (2013) 153 – 162.

[3] A sulfur–carbon composite for lithium/sulfur battery based on activated vapor-grown carbon fiber, Solid State Ionics 238 (0) (2013) 44 – 49.

[4] J. Schuster, G. He, B. Mandlmeier, T. Yim, K. T. Lee, T. Bein, L. F. Nazar, Spherical ordered mesoporous carbon nanoparticles with high porosity for lithium–sulfur batteries, Angewandte Chemie International Edition 51 (15).

[5] N. Jayaprakash, J. Shen, S. S. Moganty, A. Corona, L. A. Archer, Porous hollow carbon@sulfur composites for high-power lithium–sulfur batteries, Angewandte Chemie 123 (26).

[6] G. Zheng, Y. Yang, J. J. Cha, S. S. Hong, Y. Cui, Hollow carbon nanofiber-encapsulated sulfur cathodes for high specific capacity rechargeable lithium batteries, Nano Letters 11 (10) (2011) 4462–4467.

[7] P. G. AU Bruce, S. A. Freunberger, L. J. Hardwick, J.-M. Tarascon, Li-o2 and li-s batteries with high energy storage, Nat Mater 11.

[8] S. Xin, L. Gu, N.-H. Zhao, Y.-X. Yin, L.-J. Zhou, Y.-G. Guo, L.-J. Wan, Smaller sulfur molecules promise better lithium–sulfur batteries, Journal of the American Chemical Society 134 (45) (2012) 18510–18513.

[9] H. Wang, Y. Yang, Y. Liang, J. T. Robinson, Y. Li, A. Jackson, Y. Cui, H. Dai, Graphene-wrapped sulfur particles as a rechargeable lithium–sulfur battery cathode material with high capacity and cycling stability, Nano Letters 11 (7) (2011) 2644–2647.

[10] R. Elazari, G. Salitra, A. Garsuch, A. Panchenko, D. Aurbach, Sulfur-impregnated activated carbon fiber cloth as a binder-free cathode for rechargeable li-s batteries, Advanced Materials 23 (47).

[11] L. Ji, M. Rao, S. Aloni, L. Wang, E. J. Cairns, Y. Zhang, Porous carbon nanofiber-sulfur composite electrodes for lithium/sulfur cells, Energy Environ. Sci. 4 (2011) 5053–5059.

[12] Nano-carbon/sulfur composite cathode materials with carbon nanofiber as electrical conductor for advanced secondary lithium/sulfur cells, Journal of Power Sources 205 (0) (2012) 474 – 478.

[13] Amorphous helical carbon nanofibers synthesized at low temperature and their elasticity and processablity, Solid State Communications 138 (1) (2006) 5 – 8.

[14] M. Kumar, Y. Ando, Chemical vapor deposition of carbon nanotubes: A review on growth mechanism and mass production, Journal of Nanoscience and Nanotechnology 10 (6) (2010-06-01T00:00:00) 3739–3758.

[15] F. Nitze, Synthesis and characterization of palladium based carbon nanostrucure-composites and their clean-energy application, Ph.D. thesis, Umeå University.

[16] Carbon nanotubes and helical carbon nanofibers grown by chemical vapour deposition on {C60} fullerene supported pd nanoparticles, Carbon 49 (4) (2011) 1101 – 1107.

[17] A. A. Teh, R. Ahmad, M. Kara, M. Rusop, Z. Awang, The effect of ammonia on carbon nanotube growth using simple thermal chemical vapour deposition, Journal of Nanoscience and Nanotechnology 12 (10) (2012-10-01T00:00:00) 8201–8204.

[18] R. A. Segura, S. Hevia, P. Häberle, Growth of carbon nanostructures using a pd-based catalyst, Journal of Nanoscience and Nanotechnology 11 (11) (2011-11-01T00:00:00) 10036–10046.

[19] M. G. Roop Chand Bansal, Activated Carbon Adsorption, Taylor and Francis Group.

[20] Activation of coal tar pitch carbon fibres: Physical activation vs. chemical activation, Carbon 42 (7) (2004) 1367 – 1370, carbon '03 Conference.

[21] F. R. R. Harry Marsh, Activated Carbon, Elsevier.

[22] Understanding chemical reactions between carbons and naoh and koh: An insight into the chemical activation mechanism, Carbon 41 (2) (2003) 267 – 275.

[23] C. B. C. David B. Williams, Transmission Electron Microscopy, Springer Science + Business Media, LLC.

[24] R. Erni, M. D. Rossell, C. Kisielowski, U. Dahmen, Atomic-resolution imaging with a sub-50-pm electron probe, Phys. Rev. Lett. 102 (2009) 096101.

[25] S. Brunauer, P. H. Emmett, E. Teller, Adsorption of gases in multimolecular layers, Journal of the American Chemical Society 60 (2) (1938) 309–319.

[26] E. P. Barrett, L. G. Joyner, P. P. Halenda, The determination of pore volume and area distributions in porous substances. i. computations from nitrogen isotherms, Journal of the American Chemical Society 73 (1) (1951) 373–380.

[27] {KOH} activation of carbon nanofibers, Carbon 42 (8–9) (2004) 1723 – 1729.

[28] Ordered mesoporous carbon/sulfur nanocomposite of high performances as cathode for lithium–sulfur battery, Electrochimica Acta 56 (26) (2011) 9549 – 9555, {ELECTROCHEMICAL} {MICRO} & NANO-SYSTEM {TECHNOLOGIES}.

[29] Pdo/pd system equilibrium phase diagram under a gas mixture of oxygen and nitrogen, Journal of Phase Equilibria 23 (3).

[30] Electrochemical properties of the soluble reduction products in rechargeable li/s battery, Journal of Power Sources 195 (9) (2010) 2945 – 2949.

[31] Improvement of cycle property of sulfur electrode for lithium/sulfur battery, Journal of Alloys and Compounds 449 (1–2) (2008) 313 – 316, the First International Symposium on Functional Materials (ISFM2005).

[32] J. Guo, Y. Xu, C. Wang, Sulfur-impregnated disordered carbon nanotubes cathode for lithium–sulfur batteries, Nano Letters 11 (10) (2011) 4288–4294.